ANNUAL REPORT TO THE

LASER COMMITTEE 1994

5 April 1993 to 4 April 1994

CENTRAL LASER FACILITY
RUTHERFORD APPLETON LABORATORY
CHILTON
OXON
OX11 0QX

Telephone 0235 821900
Telefax 0235 445888

Rutherford Appleton Laboratory Report RAL-94-042

The cover illustrates *ECO RV* restriction enzyme bound to the specific site of a DNA strand prior to genetic modification, see page 203.

ISBN 0902376055

DRAL is part of the Engineering and Physical Sciences Research Council

MEASUREMENT OF ELECTRON DENSITY DISTRIBUTION IN LONG SCALELENGTH PLASMAS

L.A.Gizzi, D.Giulietti, A.Giulietti, T.Afshar-rad[1], S.M.Viana[1], O.Willi [1].

Istituto di Fisica Atomica e Molecolare, Pisa, Italy.

[1] The Blackett Laboratory, Imperial College of Science, Technology and Medicine, London, UK.

INTRODUCTION

Interferometric techniques can be used to measure the electron density distribution of a plasma as well as its temporal evolution. A fringe pattern is generated by an interferometer which gives the phase shift induced on the probe beam by the plasma and integrated along the line of sight of the interferometer. With appropriate assumptions on the symmetry of the plasma, Abel inversion allows the density distribution to be obtained from the phase shift distribution. A detailed experimental investigation was performed[1] on long scalelength plasmas produced from laser irradiation of thin Al disks. A wide range of diagnostic techniques was employed in order to characterise the plasma in terms of electron density and temperature[2]. In particular, an extensive analysis[3] of interferometric measurements has been carried out using advanced techniques[4] based on the Fourier analysis and the results are summarised here.

EXPERIMENTAL SET-UP

The long scalelength plasmas were produced at the SERC Central Laser Facility using four 600 ps, 1.053 μm beams of the Vulcan laser, focused f/10 on a 400 μm diameter Al dot targets at an irradiance from 3 to 6×10^{13}W/cm^2 on each side of the target. A 100 ps (FWHM), 1.053 μm beam of the Vulcan laser was frequency doubled, delayed and used as a probe beam for interferometric measurements in a line of view parallel to the target plane. A Nomarski-like interferometer[5] was employed in order to measure the plasma induced phase shift at various delays relative to the peak of the heating pulses. It was found that, under analogous experimental conditions, interferograms were highly reproducible shot by shot. Fig.1 shows a representative interferogram taken 4.3 ns after the peak of the heating pulses.

INTERFEROMETRY: BASIC PRINCIPLES

The fringe pattern produced by the interferometer is the result of interference between a beam which has propagated through the plasma and an unperturbed reference beam, both beams originating from the same laser source. If the electron density n_e is much smaller than the critical density, n_c at the probe wavelength, one can assume that bending effects are negligible, that is the probe beam propagates through the plasma in a straight line. In this case the phase difference between these two beams in a given position (x,z) of an output plane of the interferometer perpendicular to the probe beam is

$$\Delta\varphi(x,z) = \frac{2\pi}{\lambda_p}\left(\int_{-L/2}^{L/2}\left(\varepsilon(x,y,z)-1\right)dy\right) \qquad (1)$$

where λ_p is the probe beam wavelength, ε is the plasma refractive index, L is the total path-length greater than the plasma extent along y.

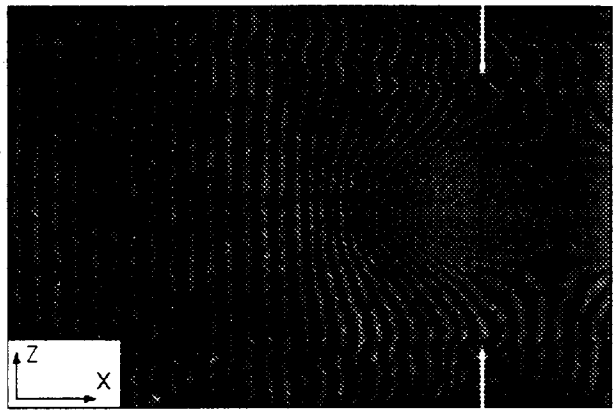

Fig.1. Interferogram of the preformed plasma taken 4.3 ns after the peak of the heating laser pulses. The intensity on each side of the target was 4.2×10^{13} W/cm^2. The position of the target is indicated by the arrows.

Considering that $n_e \ll n_c$, and assuming cylindrical symmetry of the plasma around the axis perpendicular to the target and passing through its centre, the phase shift can be written in terms of the radial co-ordinate, i.e. the distance from the symmetry axis

$$\Delta\varphi_{x_o}(z) = -\frac{e^2\lambda_p}{m_e c^2}\left(\int_z^{r_o}\frac{n_e(r)\ r\ dr}{\sqrt{r^2-z^2}}\right) \qquad (2)$$

where the usual symbols have been adopted for the electron mass and charge, and the speed of light. Eq.2 has the typical form of the Abel integral equation and can therefore be inverted to give

$$n_e(r,x) = -\frac{m_e c^2}{\pi e^2\lambda_p}\int_r^{r_o}\frac{\partial\Delta\varphi(x,z)}{\partial z}\frac{dz}{\sqrt{z^2-r^2}} \qquad (3)$$

which gives the radial distribution of the electron density in terms of the phase shift induced by the plasma, integrated along a direction perpendicular to the symmetry axis. In order to detect this phase shift a small angle is introduced by the interferometer between the probe beam and the reference beam so that, in absence of plasma, a pattern of parallel fringes is generated. The phase shift introduced by the plasma is then evaluated by measuring the displacement of the fringes from their unperturbed position. By counting the number of fringes crossed moving along z one can obtain a sampling of $\Delta\varphi$ for a given distance from the target plane. This set of data can be fitted and introduced in Eq.3 in order to calculate the electron density. However this procedure, typically used in the past, is subjected to a number of uncertainties introduced by the small number of data typically available to build $\Delta\varphi$ and by the particular choice of the fitting function. Moreover, the sensitivity of this technique is basically limited to one fringe shift which, as will be clear later, would strongly limit the effectiveness of the interferometric method itself,

capable of a much better resolution. The use of the Fourier transform method in the analysis of the interferograms allows a much more direct approach to the problem, free from the uncertainties evidenced above and easy to implement with simple numerical techniques.

FOURIER TECHNIQUE

The intensity of the fringe pattern produced by the interferometer on the output plane of the interferometer in presence of plasma can be written as

$$I(x,z) = a + b\cos[2\pi f_u x + \Delta\varphi] \qquad (4)$$

where a 1:1 plasma to image magnification has been assumed. In this equation $a(x,z)$ and $b(x,z)$ account for non-uniformities of the background intensity and fringe visibility, f_u is the spatial frequency of the unperturbed fringe pattern, i.e. the number of fringes per unit length on the output plane, $\Delta\varphi(x,z)$ is the phase shift induced by the plasma. It has been shown[6] that, by means of the Fourier analysis, the intensity $I(x,z)$ can be processed in order to directly obtain the phase shift. By expressing the cosine function in terms of the exponential function Eq.4 becomes

$$I(x,z) = a + [c\exp(2\pi i f_u x) + c.c.] \qquad (5)$$

where $c(x,z) = (1/2)\,b\exp[i\,\Delta\varphi]$ and its complex conjugate $c^*(x,z)$ carry all the information relative to $\Delta\varphi$. According to the definition of logarithm of a complex number one can verify that

$$\log c = \log[(1/2)b] + i\,\Delta\varphi. \qquad (6)$$

that is the phase shift can therefore be obtained taking the imaginary part of the complex logarithm of c. On the other hand, if we take the Fourier transform of Eq.5 with respect to x we obtain, for a fixed z

$$F_I(f) = F_a(f) + F_c(f - f_u) + F_c^*(f + f_u) \qquad (7)$$

where $F_a(f)$ is the Fourier transform of the background intensity along x and $F_c(f - f_u)$ and $F_c^*(f + f_u)$ are the Fourier transforms of the two terms containing $\Delta\varphi$. If the scalelength of typical non-uniformities of the background intensity along x is large compared to the fringe frequency, then the contribution of F_c to the total Fourier spectrum of Eq.7 will result well separated by the contribution due to the background intensity non-uniformities. In this case $F_c(f - f_u)$ can be extracted from the spectrum, shifted by f_u along the frequency axis toward the origin, in order to obtain $F_c(f)$, and inverse Fourier transformed to obtain c.

The interferogram of Fig.1 was digitised with the two scanning directions set along x and z respectively. The optical density of the film was converted into intensity and stored in a two-dimensional array. A fast Fourier transform (FFT) of the intensity distribution along the direction perpendicular to the fringes, i.e. along x was performed for each position along z. The three components of the Fourier spectrum given by Eq.7 are clearly visible in the image of Fig.2 where the modulus of the Fourier transform of the interferogram of the plasma of Fig.1, is shown as a grey-scale distribution.

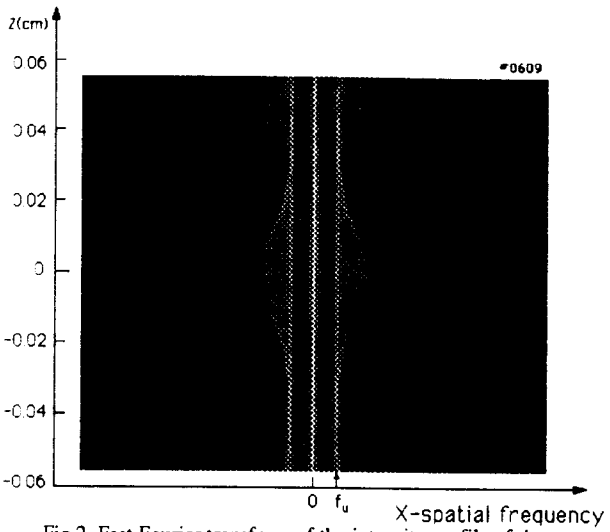

Fig.2. Fast Fourier transform of the intensity profile of the interferogram of Fig.1. The natural logarithm of the modulus is shown as a grey-scale image.

The two side components symmetric to the *zero* frequency are relative to the fringe pattern while the central, strong component accounts for the low spatial frequency variations of the background intensity.

According to Eq.6, the imaginary part of the complex logarithm of $c(x,z)$ will finally give the phase distribution $\Delta\varphi(x,z)$ that is still locally indeterminate by a factor of 2π resulting from the use of an inverse trigonometric function to obtain the argument of $c(x,z)$. However this indetermination can be solved by setting an appropriate algorithm able to detect and compensate jumps in the phase shift.

Fig.3 shows a 3D shaded surface of the phase shift distribution generated by the preformed plasma 4.3 ns after the peak of the heating pulses. According to Eq.3, the phase distributions of Fig.3 can be inverted to determine the electron density distribution.

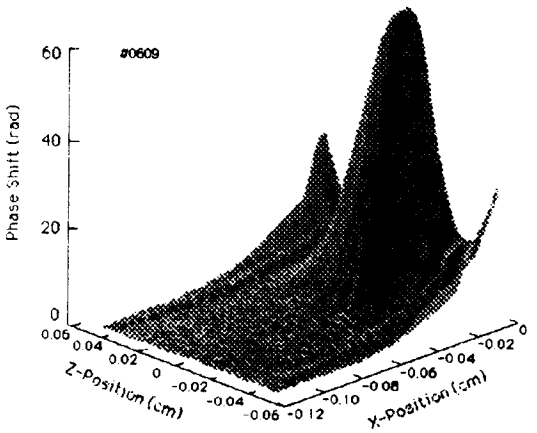

Fig.3. 3D shaded surface of the phase shift distribution obtained from the interferogram of Fig.1 using a Fourier based technique (see text).

The integral in the equation has been solved numerically using a corrected composite trapezoid rule. Due to the large amount of phase data points available, typically

512x512, the integral could be performed directly on the data itself, without polynomial fitting. A contour plot of the density profile obtained from Abel inversion of the phase shift of Fig.3 is shown in Fig.4. The contour levels are labelled in terms of the critical density at 1 μm. Consistently with the assumption of cylindrical symmetry, the z-co-ordinate of Fig.3 has been replaced by the *radial* co-ordinate.

SENSITIVITY TO DENSITY INHOMOGENEITIES

The analysis of interferograms with the Fourier technique results in a substantial improvement of the sensitivity to small scale non-uniformities in the density distribution. The fringe shift recorded on film is the result of spatial integration along the line of sight of the interferometer, the sensitivity of our measurements to local density inhomogeneities depends upon their scalelength as well as their amplitude.

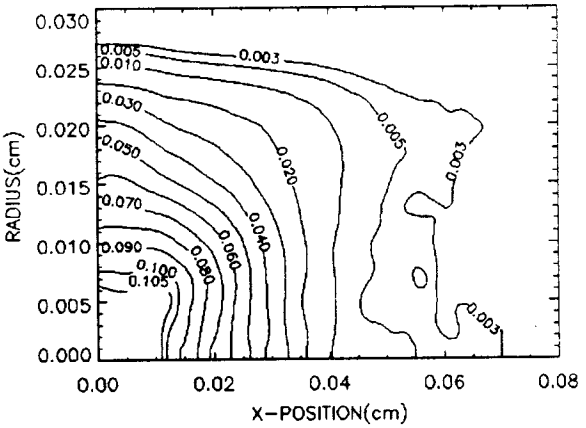

Fig.4. Contour plot of the electron density profile of the plasma 4.3 ns after the peak of the heating pulses as obtained from Abel inversion of the phase shift distribution of Fig.3. Contour levels are labelled in terms of the critical density at 1.053μm.

According to Eq.2 the phase shift induced by the plasma is linear with the density itself. The contribution of a local density inhomogeneity to the total phase shift $\delta\varphi$ has been evaluated assuming a density inhomogeneity along the line of sight at a given position (x_o, z_o) on the output plane of the interferometer given by

$$\delta n_e(x,y,z) = a\, n_{c@1\mu m} \exp(-y^2/w^2) \qquad (8)$$

where a is the amplitude of the density perturbation in units of the critical density at 1 μm, $n_{c@1\mu m}$ and w is the scalelength of the perturbation.

The phase shift $\delta\varphi$ must be compared with the minimum phase shift which can be experimentally detected. With the use of the Fourier technique described here the uncertainty in the phase shift arises from the non-linearity in the response of the detector used to record the interferogram. It has been shown in Ref.6 that such non-linearity would give rise to high frequency noise in the phase distribution. An estimate of the importance of this effect can be made from the contour plot of the phase shift of Fig.3 which is reported in Fig.5. It shows that the contour curves are perturbed by a high frequency noise. This effect leads to an uncertainty typically of the order of 0.5 rad that is less than one tenth of a fringe separation.

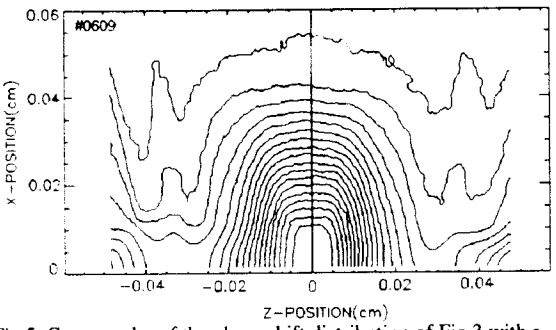

Fig.5. Contour plot of the phase shift distribution of Fig.3 with a contour interval of π, the uppermost curve corresponding to $\varphi=\pi$.

Consequently, according to Eqs.8, a single electron density perturbation along the line of sight with a scalelength of 20 μm will be detected as long as the corresponding amplitude of density fluctuation is greater than $0.01\, n_{c@1\mu m}$. This limit becomes $0.025\, n_{c@1\mu m}$ for a 10 μm scalelength perturbation.

Incidentally we observe that this procedure can also be used to determine the lowest electron density which can be detected for a given plasma extent along the line of sight of the interferometer. Assuming a plasma extent of the order of the target diameter, that is 400 μm, the uncertainty of 0.5 rad on the phase distribution mentioned above gives a lower limit to the detectable density of $\approx 10^{-3}\, n_{c@1\mu m}$ which is consistent with the measured limit given by Fig.4.

The sensitivity of the interferometric measurements to small scale density non-uniformities is a fundamental step for a correct interpretation of interaction experiments. From the point of view of the filamentation instability, for example, this study indicates that perturbations in the bulk of the plasma in the range of scalelengths of 10-20 μm, are typically characterised by $\delta n_e/n_e < 0.2$. The plasma studied here can be therefore be considered substantially free from density inhomogeneities which can efficiently initiate the instability.

REFERENCES

1 L.A.Gizzi, T.Afshar-Rad, V.Biancalana, P.Chessa, A.Giulietti, D.Giulietti, E.Schifano, S.M.Viana, O.Willi, RAL Annual Report, **RAL-92-020**, p.34, 1993.

2 L. A.Gizzi, T.Afshar-Rad, V. Biancalana, P.Chessa, A.Giulietti, D.Giulietti, E. Schifano, S. M. Viana, O. Willi, "22nd ECLIM", Paris, May. 10-14, 1993.

3 L.A.Gizzi, D.Giulietti, A.Giulietti, T.Afshar-Rad, V.Biancalana, P.Chessa, C.Danson, E.Schifano, S.M.Viana, O.Willi, accepted for publication, Phys.Rev. E (1994).

4 M.Takeda, H. Ina, S. Kobayaski, J. Opt. Soc. Am. **72**, 156 (1982).

5 M.G.Nomarski, Journal de la Physique et le Radium, **16**, 95 (1955); R.Benattar, C. Popovics, R. Siegel Rev. Sci. Instrum. **50**, 1583 (1979); O. Willi, in Laser-Plasma Interaction 4, Proceedings of XXXV SUSSP, St. Andrews, 1988.

6 Keith. A. Nugent, Appl. Optics **24**, 3101 (1985).